# Community-Oriented Data Integration and Communication Framework for Streamflow Forecast Models and Flood Inundation Map Products

Kento Sugiyama[1,2], Carlos Erazo Ramirez[3,4], Ibrahim Demir[3,4]

[1] College of Liberal Arts and Sciences, University of Iowa, Iowa City, IA
[2] West Senior High School, Iowa City, IA
[3] River-Coastal Science and Engineering, Tulane University, New Orleans, LA
[4] ByWater Institute, Tulane University, New Orleans, LA

## Abstract

Access to critical flood risk information is often limited by expert-driven workflows that require specialized software, representing a barrier to stakeholder engagement and effective science communication. This study presents a generalized web-based framework that integrates federal datasets for real-time scenario-based flood forecasting and mapping at the CONUS scale. By leveraging state-of-the-art client-side technologies, including WebAssembly, Web Workers, and IndexedDB, we developed an on-demand geoprocessing framework for flood inundation maps directly in the browser. The flood maps can be generated based on flood forecast outputs from the National Water Model and products from the Office of Water Prediction Flood Inundation Mapping. The framework also provides FEMA HAZUS damage assessment capabilities applied to property data from the National Structure Inventory. The platform's capabilities are demonstrated through a case study of the 2019 Midwestern Floods, showcasing its value as an accessible and scalable tool for emergency managers, planners, and communities to assess flood risks.

**Keywords:** flood maps, flood forecasting, web framework, visualization, damage estimation

## Software and Data Availability

| | |
|---|---|
| Software | Community-Oriented Flood Information System (CoFIS) |
| Developer | Kento Sugiyama |
| Contact Information | cerazoramirez@tulane.edu |
| First Available | 2025 |
| Programming Language | HTML, CSS, JS, WebAssembly |
| Cost | Free |
| Software Availability | https://hydrointelligence.github.io/apps/nwcapp/ |

## 1. Introduction

Flooding is among the most damaging and prevalent natural hazards, resulting in significant economic and infrastructure losses worldwide. In the United States, damages amount to tens of billions of dollars annually during flood season (Wing et al., 2018) and are likely to intensify as extreme weather events increase in frequency (Trenberth et al., 2015; Seneviratne et al., 2021). At the same time, ongoing urban expansion further concentrates on people and assets in flood-prone areas, thereby increasing the risks of human losses (IPCC, 2023).

Effective flood mitigation and response are built upon a foundation of robust hydrological modeling, which is essential for understanding and predicting the complex interactions between water and the landscape (Teng et al., 2017; Cikmaz et al., 2025). Modern flood analysis integrates a variety of geospatial datasets to link physical processes with spatial contexts. Digital Elevation Models (DEMs) provide the fundamental topographic data for delineating watersheds and flow paths, while hydrographic datasets such as the National Hydrography Dataset Plus (NHDPlus) offer a detailed representation of the nation's stream network (Demiray et al., 2021). Tools such as GDAL (Geospatial Data Abstraction Library) are crucial for transforming these geospatial datasets in preparation for subsequent analyses (Gesch et al., 2002; Moore et al., 2019; Brakebill et al., 2020).

Traditionally, these processes rely on powerful desktop software and tools, such as HEC-RAS, ArcGIS, and QGIS, which enable detailed hydraulic simulations but often require significant computational resources and expertise (Samela et al., 2018; Qian et al., 2024; Tsegaye et al., 2024). More recently, a computationally efficient methodology called Height Above Nearest Drainage (HAND) has gained popularity for large-scale flood inundation mapping (FIM) using moderate to coarse resolution elevation data, typically 10 meters and above (Nobre et al., 2011; Li et al., 2023). By leveraging a relative elevation model framework that quantifies the vertical distance from the nearest drainage channel, HAND can achieve accuracy comparable to traditional methods but with a significantly lower computational cost, making it highly suitable for rapid, scenario-based assessments (Johnson et al., 2019; Aristizabal et al., 2024; Baruah et al., 2025a; NOAA OWP, 2025). The development of analysis-ready datasets from the National Water Center presents a significant opportunity to advance flood map generation using this computationally efficient HAND methodology.

Despite these advances, the practice of flood risk assessment remains constrained by expert-driven workflows and specialized software, creating a significant barrier that limits the accessibility of critical flood risk information for non-technical stakeholders, such as emergency managers, urban planners, and community members. In response, a variety of web-based platforms have emerged to democratize access to water resources data and modeling tools. Platforms such as the Iowa Flood Information System (Demir & Krajewski, 2013) and frameworks for urban flood analysis (Alabbad et al., 2023, 2024; Sufi et al., 2025) provide valuable web-based decision-support tools. On a larger scale, platforms such as Google Earth Engine, Tethys, and CUAHSI HydroShare utilize open-source cloud infrastructure to provide access to vast geospatial datasets and models (DeVries et al., 2020; Gorelick et al., 2017; Hales et al., 2022; Horsburgh et al., 2015;

Nelson et al., 2019). However, these powerful platforms often rely on substantial server-side infrastructure, which can introduce significant computational costs, data transfer fees, and a dependency on persistent internet connectivity.

A promising alternative is to explore the use of client-side technologies, which enable direct hydrologic analysis in the user's web browser (Sit et al., 2021). Foundational work demonstrating this potential includes the development of the Hillslope Link Model (HLM), a simulation engine for rainfall-runoff modeling written in JavaScript (Ewing et al., 2022). This client-side model facilitates its use in hydrological education and research. Moreover, interactive gaming engines (Emiroglu et al., 2025; Demiray et al., 2025) strongly highlight the use of advanced visualization techniques and analytics directly through a standard web browser. More recent advances in client-side technologies, such as WebAssembly, WebGPU, and Web Workers, have enabled even more complex analyses. Sit et al. (2019) developed a client-side watershed deliberation algorithm using JavaScript, WebAssembly, and WebGL.

The HydroLang framework (Erazo Ramirez et al., 2021; 2022) further advanced this paradigm by providing a comprehensive suite of tools and declarative interfaces for client-side hydrological analysis. In addition, libraries such as HydroCompute (Ramirez et al., 2024) have demonstrated the power of this approach for hydrological computations, achieving performance comparable to that of desktop applications. Additionally, work by Hu & Demir (2021) on client-side flood inundation mapping established the feasibility of real-time flood modeling in the browser by compiling a C++ implementation of the HAND algorithm to WebAssembly. Li & Demir (2022) later developed a comprehensive platform utilizing this methodology, which included tools for generating custom maps and conducting analysis. These studies were instrumental in proving the technical feasibility of client-side geospatial processing and flood modeling.

However, existing studies have not leveraged client-side technologies to create an operational platform that fully integrates national-scale datasets with forecast models for reliable, scenario-based flood inundation mapping across the continental United States. Therefore, this study addresses this gap through the development of a web-based platform that leverages client-side processing for real-time flood inundation mapping. Our approach connects the Office of Water Prediction's (OWP) high-quality relative elevation models with discharge predictions from the National Water Model (NWM), enabling dependable, on-demand inundation mapping for any river reach in the continental United States. By building on a nationally consistent hydrofabric (Blodgett & Johnson, 2025), this platform provides emergency managers, planners, and community stakeholders with immediate and intuitive access to flood modeling capabilities. In this paper, we present the following capabilities: (a) the client-side architecture for integrating heterogeneous federal datasets; (b) demonstrate its capabilities for real-time, scenario-based flood modeling and infrastructure impact assessment; and (c) evaluate the platform's accuracy and performance through a case study of the 2019 Midwestern floods.

## 2. Scenario-Based Flood Inundation Mapping Framework

### 2.1. System Overview

This framework integrates interactive flood scenario generation, historical and forecast model outputs, and on-the-fly infrastructure damage estimations into a single, cohesive user interface. By synthesizing heterogeneous federal datasets, the system overcomes common barriers of data fragmentation and accessibility, enabling comprehensive flood inundation mapping and impact assessment through a unified platform (Table S1). The platform initially displays watershed features at various scales, ranging from HUC-2 to HUC-12. Users can then create flood inundation maps at the river reach level by directly controlling stage values or through real-time and retrospective predictions from the National Water Model (NWM). A technical overview of the platform, including web technologies, data sources, and analysis features, is presented in Figure 1. The analysis features, scenario-based flood extents and infrastructure assessment, are explained in Section 3.

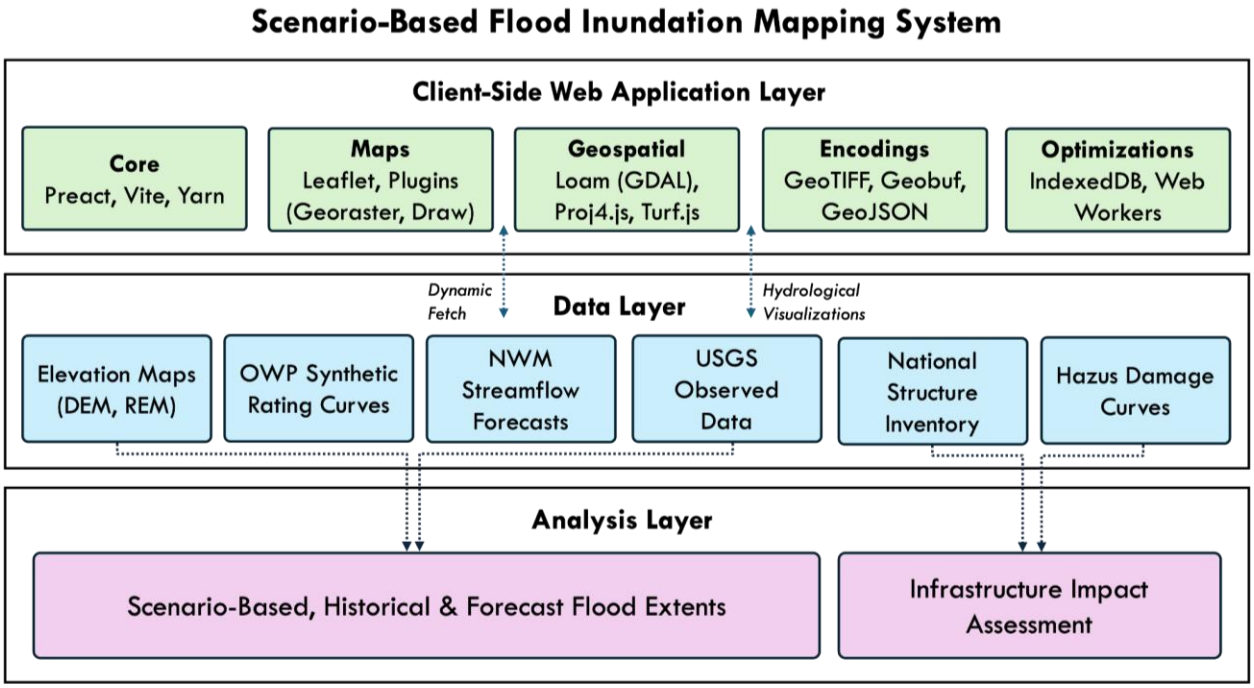


Figure 1. Technical overview and components of the framework.

The platform is built on a modern front-end architecture using Preact and the Vite build tool for optimal performance, with Tailwind CSS for consistent styling (Miller, 2025; Wathan, 2024; You, 2025). This ensures a high degree of accessibility and performance across all modern web browsers. The application is primarily driven by user interaction with the mapping engine, providing real-time updates through visualizations of various data formats. Interactive mapping is implemented using the Leaflet library (Agafonkin, 2023), with a simple base map (CARTO, 2024) and specialized layers for visualizing hydrological data. Leaflet was chosen due to its open-source nature and extensibility through community-driven packages and implementations. For raster data

visualization, the system utilizes the *georaster-layer-for-leaflet* package (Dufour et al., 2022), incorporating custom pixel-to-color mapping functions for the representation of elevation and flood depth. The Leaflet mapping architecture supports diverse visualization requirements, including point-based markers for USGS gauge stations, real-time flood inundation raster overlays, and integrated search functionality with spatial context awareness.

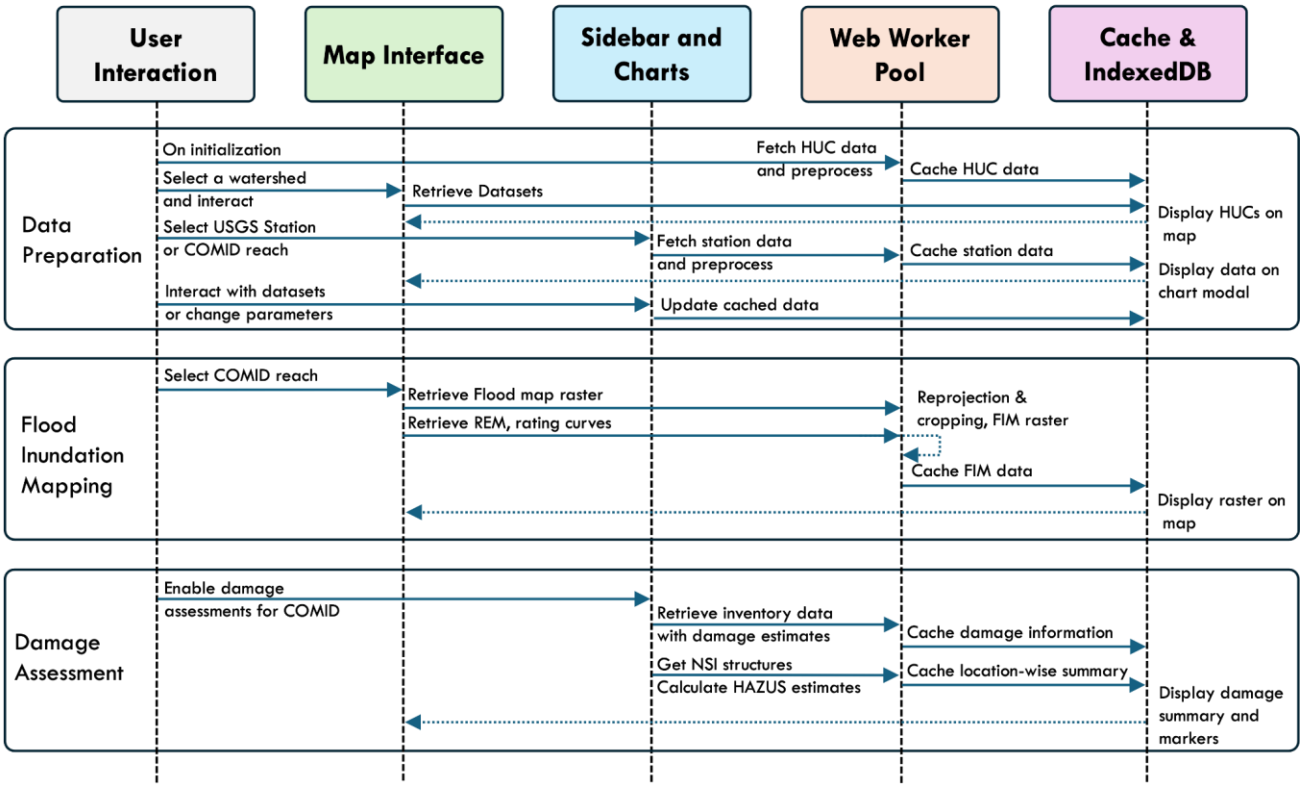


Figure 2. System workflow sequence describing the data flow and processing steps from initial data preparation to flood mapping and damage assessment.

The platform operates on an entirely client-side computing architecture, ensuring high performance and a responsive user interface, without relying on server-side computational resources. The system uses Web Workers to manage asynchronous operations, preventing the main thread from freezing during intensive calculations. For efficient data management, large geospatial datasets and user-generated scenarios are cached locally in the browser using IndexedDB. A detailed description of this processing architecture, including its implementation with WebAssembly for geospatial operations, is provided in Section 3.2. Figure 2 illustrates the technical workflow through a sequence diagram, from initial data preparation to flood mapping and damage assessment.

### 2.2. Hydrological Features and Data Visualization for Analysis

The application displays watersheds by linking them through their respective HUC identifiers, as explained in Jones et al. (2009). The platform allows for hierarchical watershed views spanning

from HUC-2 to HUC-12 levels. HUC-2 catchments for the continental US are initially displayed, with finer HUC levels progressively loaded upon user interaction (Figure 3). The data for HUC-2 and HUC-4 are stored as a single GeoJSON for the continental United States, encoded into the GeoBuf format for compression (Agafonkin, 2020). For other HUC levels, the USGS Web Feature Service (WFS) server is used to obtain the vector data, enabling fast catchment loading upon request. To aid in visualization, the current HUC level is displayed as a concatenated string in the interface, allowing the users to track their navigation through the nested watershed hierarchy.

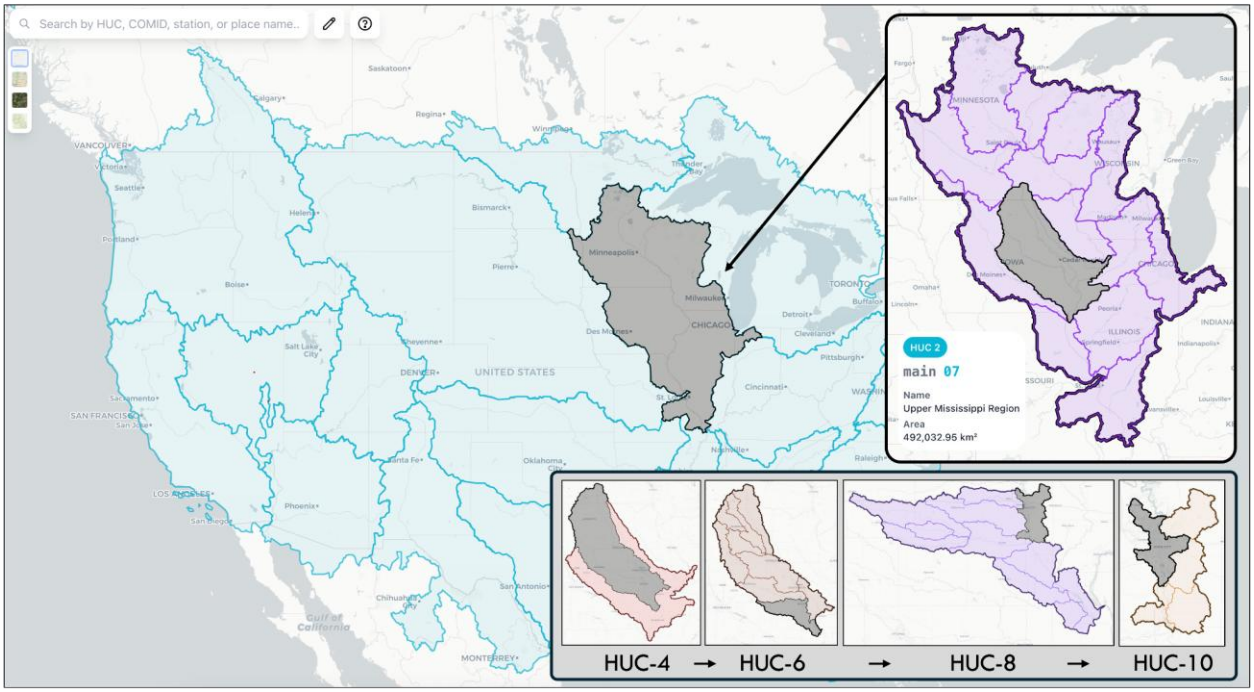


Figure 3. Example interaction of HUC-2 catchments and their corresponding subcatchments across the United States. The inset panel displays the interaction between the higher-order catchments and their children. When a HUC-2 is selected, a panel shows the current HUC level and basic properties about the watershed.

At HUC-12, hydrological features are displayed through a layer-based system (Figure 4). At this zoom level, visualization of NHDPlus flowlines and catchments (Brakebill et al., 2020), digital elevation maps (Sugarbaker et al., 2014), and USGS gauge stations (McCallum & Riskin, 2025) are made available for visualization. Within the sidebar, a FIM preparation section is included, which tracks the retrieved Relative Elevation Model (REM) raster datasets and rating curves stored in the application database at the HUC-8 level.

To aid in generating scenario-based flood maps, USGS stations are utilized to obtain observed data. Upon clicking a station, a modal with metadata panels appears, containing station information, current status, historic crests, and flood-related data. As a complement to the observed USGS discharge, the National Water Prediction Service (Cosgrove et al., 2024) 30-day observed data for discharge and water depth were used. It is worth noting that data availability differs across

gauge stations, with variations in record length, continuity, and measurement frequency. Users can also export time-series data through the modal interface.

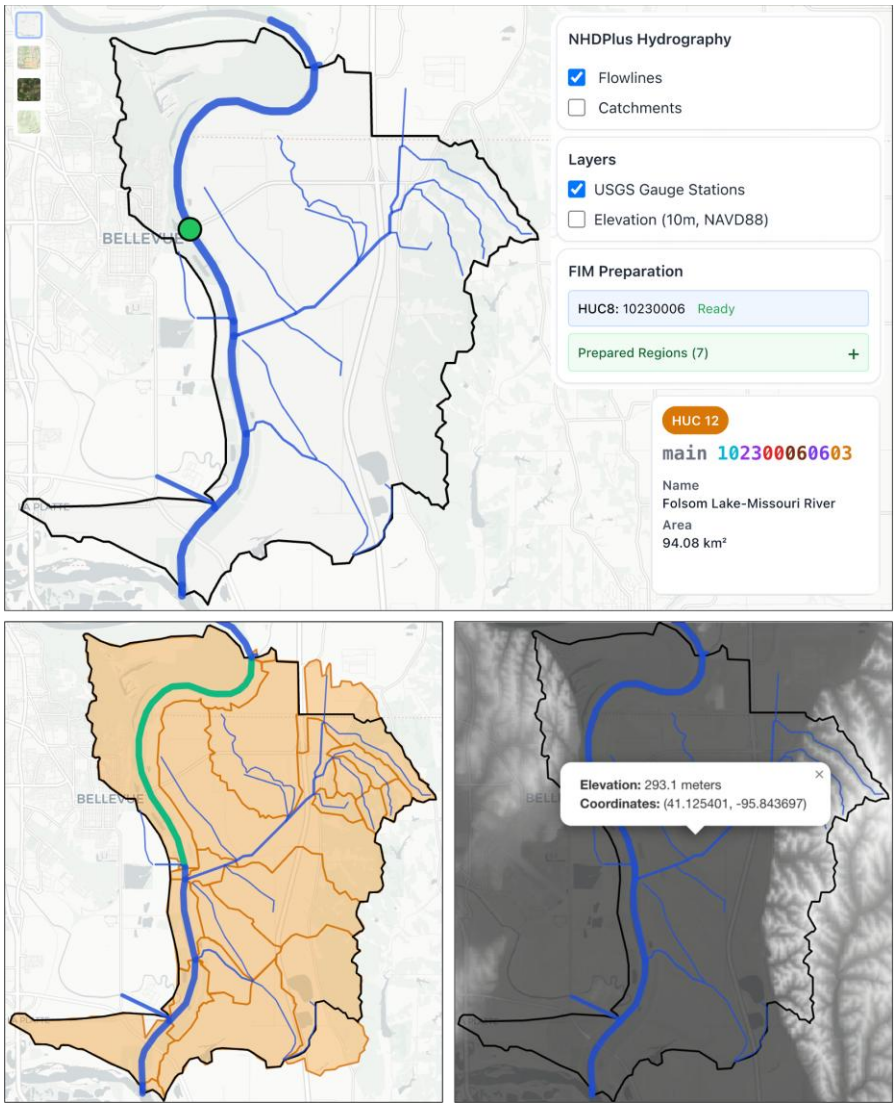


Figure 4. (Top) Example of the different hydrological features found within a HUC-12. These layers are directly controlled and manipulated through the sidebar on the right of the screen. (Bottom Left) Catchments layers shown for the HUC-12 region and (Bottom Right) Elevation layer.

At the HUC-12 level, users can select individual river reaches to display information about a specific reach using a Common Identifier (COMID) code, which is linked to the National Hydrography Dataset (Brakebill et al., 2020). On selection, the reach displays metadata, including stream names, lengths, stream orders, and drainage areas. Flowline selection enables access to time series data, along with elevation and flood maps, through specific layers in the sidebar.

As part of the prediction availability per reach, forecasts and observations are available through the National Water Model (NWM). The NWM retrospective data (Cosgrove et al., 2024) provides discharge, derived from observations and reanalysis from 1980 to 2022, with the NWM analysis assimilation providing forecasts per reach at short (24-hour), medium (10-day), and long (30-day) levels, from 2018 to present (Markert et al., 2024). Using the same approach as with the streamflow gauges, both discharge and velocity data are displayed at the COMID level. Figure 5 showcases assimilation data display for a river reach in Rock Valley, IA, during the 2024 Northwest Iowa Floods.

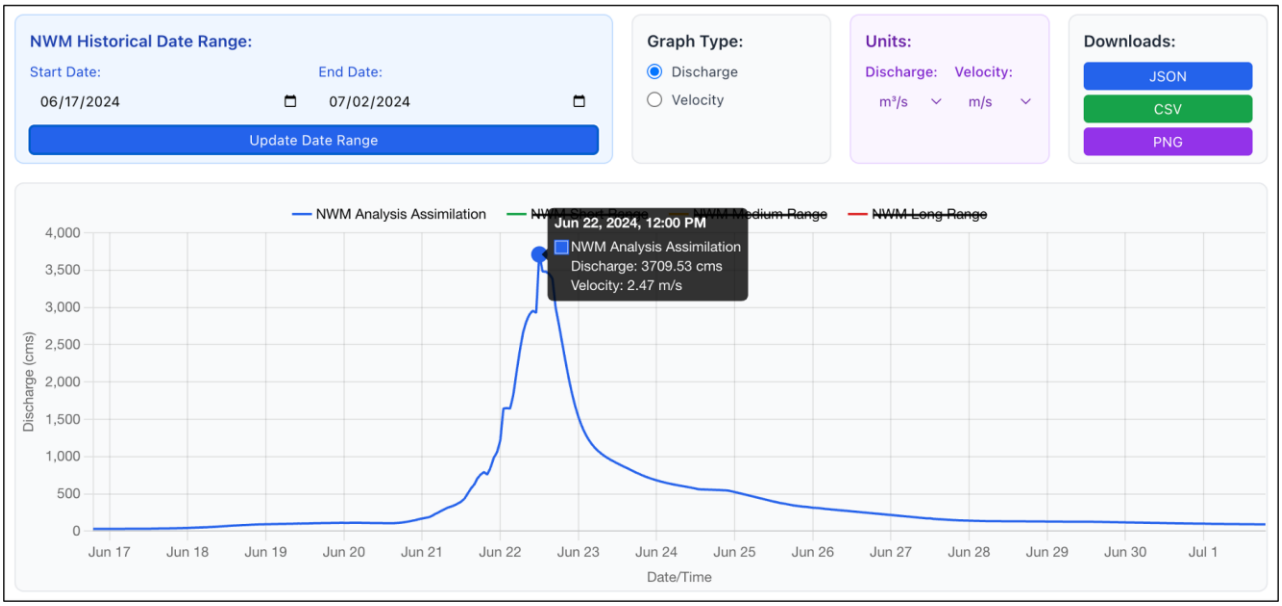


Figure 5. Analysis assimilation data from NWM simulations on the Rock River reach in Northwest Iowa at the peak of June 2024 floods.

## 3. Client-Side Processing Architecture

Within the flowline view, users can generate scenario-based maps using the Height Above Nearest Drainage (HAND) methodology (Nobre et al., 2011). This method utilizes relative elevation models (REMs) and synthetic rating curves, derived from catchment-specific hydraulic properties (Baruah et al., 2025b; NOAA Office of Water Prediction, 2025), to produce flood depth maps at the individual river reach (COMID) level. Within the platform, user-specified or model-derived discharge values are used to generate scenario inundation maps through a methodology widely adopted in both research and practice (Johnson et al., 2019; Thalakkottukara et al., 2024).

### 3.1. HAND Model Implementation

The platform implements the HAND approach through a multi-branch REM organization at the HUC-8 watershed scale. Following the OWP-HAND framework, the stream network within each HUC-8 is partitioned into continuous level paths (LPs) to reduce spurious influences from

neighboring tributaries. The mainstem LP is indexed as branch 0, and tributary LPs are numbered sequentially (Aristizabal et al., 2023).

The HAND method relies on a sequence of geospatial processing steps that transform a hydroconditioned digital elevation model (DEM) into a relative elevation model normalized to the stream network (Figure 6; adapted from Rebolho et al., 2018). The process starts with a DEM, which provides the raw terrain elevations for the catchment. From this, a drainage direction grid is computed, where each cell is assigned its steepest descent path, defining how surface water will flow across the landscape. By accumulating flow from upstream cells, drainage areas are calculated, with high accumulation values indicating channel cells.

The HAND value for each cell is then determined as the difference between its elevation and the elevation of the nearest channel thalweg cell along its drainage path. This represents the additional water depth required for inundation to occur at that cell. The resulting HAND raster forms a relative elevation model (REM) that captures the vertical distance from land surface to the river network, providing the foundation for scenario-based flood inundation mapping. All layers are precomputed by OWP-HAND (NOAA Office of Water Prediction, 2025) and organized as rasters at the HUC-8 level for efficient retrieval and application within the platform.

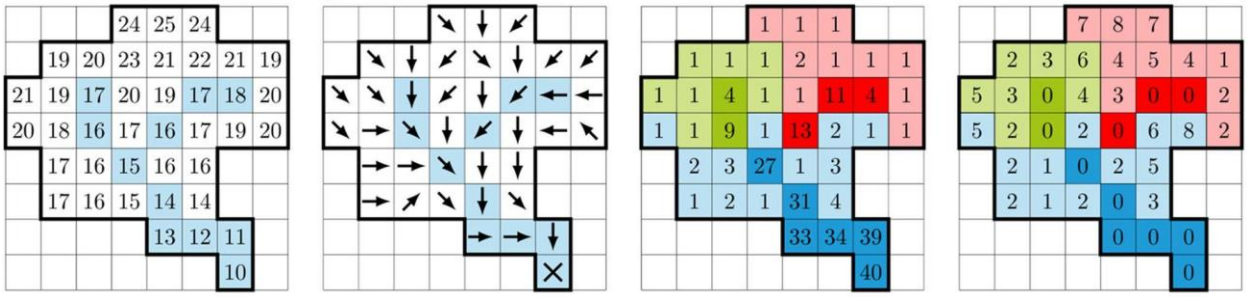


Figure 6. Schematic of HAND model calculation for FIM generation. Adapted from Rebolho et al. (2018).

Each LP is further subdivided into HydroID-defined (reach-scale) catchments. A HydroID is the unique identifier assigned in the OWP Hydrofabric to a modeling reach and its associated catchment. Because NHDPlus reaches can be split into multiple modeling units, a single COMID may correspond to several HydroIDs. Each HydroID catchment represents the drainage area contributing to its reach outlet and is the unit to which HAND elevations and hydraulic properties are applied. Reach-specific parameters, including average channel geometry, Manning's roughness, and local slope, are linked to each HydroID.

Stage values must be provided to generate flood inundation maps using the HAND model. To leverage National Water Model outputs to generate extents, stage values must be obtained by converting discharge predictions to stage values, which serve as input for the HAND model. Synthetic rating curves (SRCs) are extracted from OWP-FIM, as shown in Figure 7. These SRCs are derived using Manning's equation applied to reach-averaged channel properties and provide

the necessary relationships between modeled discharge and stage for every HydroID catchment. Once retrieved, SRCs are cached locally (in IndexedDB) to enable efficient, real-time performance during interactive scenario modeling.

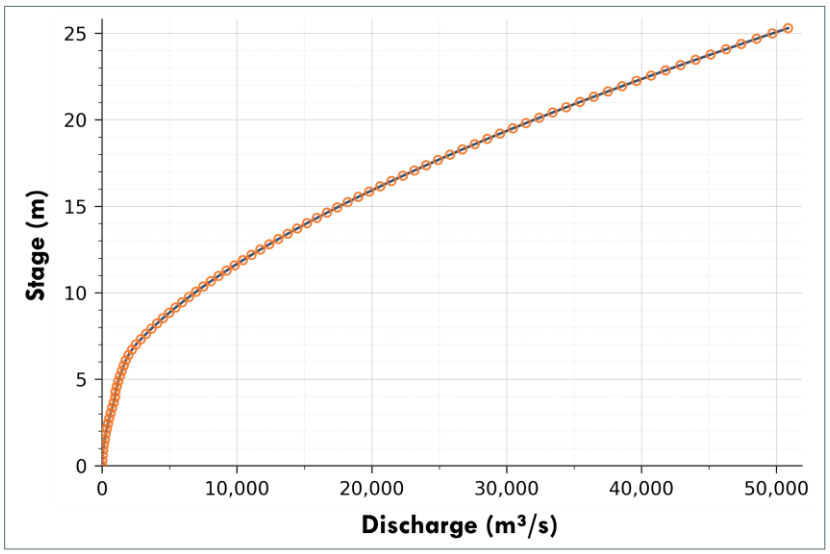


Figure 7. Stage-discharge rating curve for a catchment area 21690030 in Bellevue, Nebraska.

### 3.2. Real-Time Flood Inundation Mapping

The system provides two complementary modes for scenario development. In "master discharge" mode, a discharge value is specified once for the selected reach, and the corresponding stages for all HydroID catchments are obtained by applying their respective synthetic rating curves (SRCs). This ensures a consistent, reach-wide baseline and allows users to inspect stage values per catchment without additional input. In "individual control" mode, users can override the baseline and assign stage values individually to each HydroID catchment using interactive sliders. This functionality supports the exploration of hydrological variability along the reach, where differences in local slope, channel geometry, or Manning's roughness generate distinct inundation patterns. Both modes feature bidirectional conversion between discharge and stage via linear interpolation on the SRCs. A typical display of the flood mapping user interface is shown in Figure 8.

Integration with the National Water Model extends these capabilities by automatically converting forecast discharges into catchment-specific stages. Users can generate scenarios from retrospective NWM 3.0 (1980-2022) (Cosgrove et al., 2024), near-real-time assimilation records (2018-present), or forecast horizons of 24 hours, 10 days, and 30 days (Markert et al., 2024). The platform generates flood maps entirely in the browser environment through client-side geospatial processing. The system utilizes Geospatial Data Abstraction Library (GDAL) compiled to WebAssembly (WASM) through Loam library (Dohler, 2022), to enable web-native geospatial operations without server dependencies.

This allows for reprojection between EPSG:5070 (NAD83 Conus Albers) and EPSG:4326 (WGS84), with raster datasets stored on the client side at the HUC-8 level. In addition, Loam library crops raster datasets on the fly to include only the areas relevant to the current scenario, significantly reducing processing resources compared to processing entire HUC-8 datasets. The system maintains HUC-8-specific IndexedDB databases for caching relative elevation models, rating curves, and catchment reference raster datsets, thereby eliminating redundant data transfers across repeated analysis sessions.

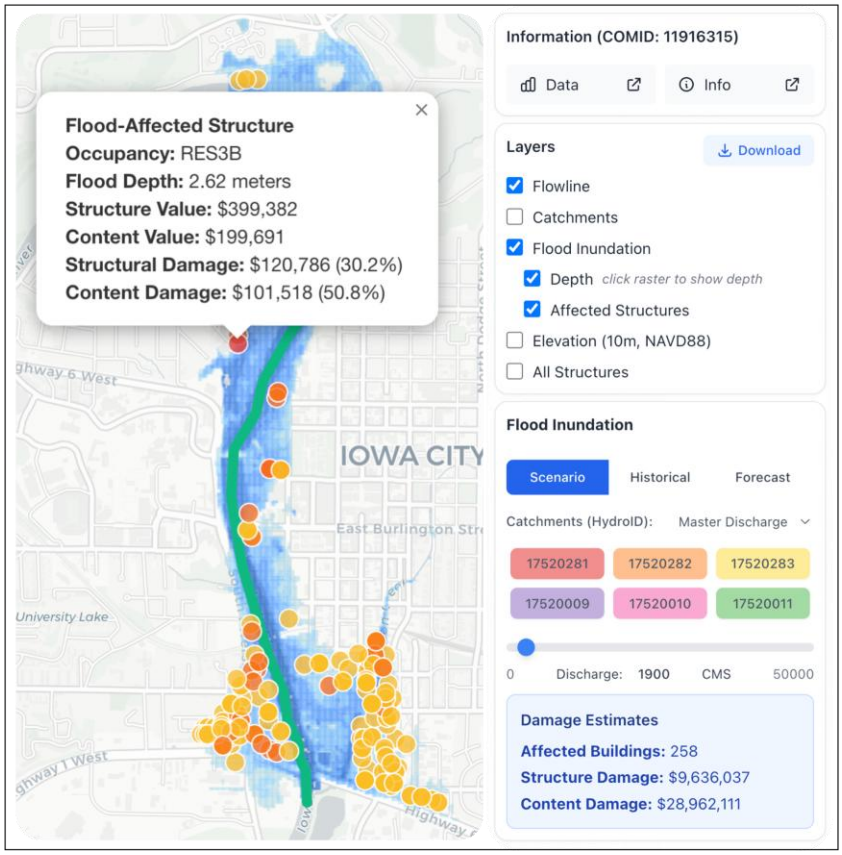


Figure 8. Flood inundation mapping user interface display with flood inundation and affected structures layers. Users can generate inundation extents through scenario-based modeling using a discharge slider or by referencing National Water Model historical and forecast values.

The architecture also employs Web Workers, concurrent processing threads, to maintain responsive user interfaces during computationally intensive operations. Raster cropping, raster mosaicking, stage-discharge conversions, and flood depth calculations execute in background threads, allowing users to continue interacting with the interface while scenarios are generated. Progress indicators provide real-time feedback on processing status, with typical scenario generation completing within seconds. The system processes flood calculations in discrete batches to manage memory utilization during extended analysis sessions.

Internally, the workflow applies the specified stage to the REM for each HydroID catchment. Flood depth at each pixel is computed as stage minus REM, and the raster datasets are mosaiced to form the inundation map. Depths are displayed on the map using a blue gradient, varied by severity (Figure S1 in supplementary material). The complete computational workflow integrating web worker spawning, raster processing, and damage calculation is presented in Figure 9. This pseudocode illustrates the systematic approach, from initial data preparation to final infrastructure impact assessment, highlighting the platform's client-side processing capabilities and optimization strategies.

**Algorithm 1** Client-Side Flood Map Generation with Multi-Branch Processing

**Require:** Discharge $Q$ (CMS), watershed HUC8, stream reach COMID
**Ensure:** Georeferenced flood depth raster $M_{geo}$

**Phase 1: Data Retrieval**
$DB \leftarrow$ IndexedDB.open($HUC8$)
$Branches \leftarrow$ getBranches($COMID$)
▷ Multi-branch framework

**Phase 2: Discharge to Stage**
**for** branch $b \in Branches$, **do**
catchment $h \in b$
$S_h \leftarrow$ interpolate($Q$, $DB.ratingCurve(h)$)
▷ Linear interpolation
**end for**

**Phase 3: Optimal Bounds**
$B_{optimal} \leftarrow \bigcup_{h \in H} DB.bounds(h)$
▷ Union of catchments
$B_{buffered} \leftarrow B_{optimal}$ +500m buffer
▷ Safety margin

**Phase 4: GDAL Raster Processing**
**for** branch $b \in Branches$ **do**
$R_{rem}(b), R_{hydroid}(b) \leftarrow DB[b]$
▷ Retrieve ArrayBuffers
$T_{rem}(b) \leftarrow$ GDAL.warp $(R_{rem}(b), B_{buffered})$
$T_{hydroid}(b) \leftarrow$ GDAL.warp $(R_{hydroid}(b), B_{buffered})$
▷ NAD83 → WGS84
**end for**

**Phase 5: Flood Depth Calc**
**for** branch $b \in Branches$ **do**
$R_{flood}(b) \leftarrow$ Float32Array($W \times H$) $.fill(-9999)$
**for** pixel $i$ in raster **do**
$h_{id} \leftarrow T_{hydroid}(b)[i]$
**if** $S_{h_{id}} > T_{rem}(b)[i]$ **then**
$R_{flood}(b)[i] \leftarrow S_{h_{id}} - T_{rem}(b)[i]$
**end if**
**end for**
**end for**

**Phase 6: Mosaicking**
$M_{geo} \leftarrow$ createGeoRaster (mosaic($\{R_{flood}(b)\}$), $B_{buffered}$)

**return** $M_{geo}$

Figure 9. Pseudocode for generating the flood inundation raster.

### 3.3. Infrastructure Impact Assessment

Building upon the flood inundation mapping capabilities discussed in Section 3.2, the platform extends scenario analysis to include comprehensive infrastructure impact assessment and economic damage estimation. This process converts raw flood depth predictions into actionable decision support by quantifying potential impacts on local infrastructure. Infrastructure impact assessment uses the National Structure Inventory (U.S. Army Corps of Engineers, 2022) to identify and characterize buildings within flood-prone areas. NSI provides comprehensive building-level data, including occupancy classifications, structural characteristics, economic valuations, and population estimates for structures across the United States. Structure discovery utilizes the

optimal bounds calculated during flood scenario generation, requesting data only within the precise extent determined by its HydroID catchments. To optimize performance during iterative scenario development, a caching strategy is employed. Upon initial selection of a river reach, all structures within the calculated optimal bounds area are downloaded and locally cached. Subsequent damage calculations occur instantly as users adjust flood scenarios, enabling real-time updates on impact assessment.

Economic impacts are quantified using damage functions from the FEMA HAZUS methodology (Alabbad et al., 2023; Scawthorn et al., 2006; Sufi et al., 2025), which provides a standardized framework for flood damage estimation. HAZUS provides empirically derived damage functions that relate flood depth to expected damage percentages for various building types, based on extensive field data and engineering analysis. These depth-damage relationships form the foundation for assessing economic impacts across diverse occupancy classifications. This damage curve implementation covers a spectrum of occupancy types, including residential (RES1-RES6), commercial (COM1-COM10), industrial (IND1-IND6), and specialized categories for agricultural, educational, government, and religious facilities. Each occupancy type maintains distinct vulnerability characteristics, which are represented in HAZUS by occupancy-specific damage curves for structure and content. Occupancy classification mapping accommodates NSI's detailed building codes by assigning them to corresponding base HAZUS categories. Multi-variant residential codes, such as "RES1-2SWB" from NSI, are mapped to base "RES1" curves, while detailed commercial subcategories use the most appropriate COM category. Linear interpolation between HAZUS curve points enables the precise calculation of damage percentages for any flood depth value.

Flood depth integration with HAZUS damage curves enables the instantaneous calculation of economic impact for each structure within affected areas (Mostafiz et al., 2021). Computational workflow samples site-specific flood depths at building footprints, applies appropriate depth-damage functions, and converts damage percentages to monetary losses using NSI-reported structure and contents valuations. Structural damage refers to physical impacts on a building's framework, foundation, and integrated systems, whereas content damage includes impacts on movable property, including furnishings, equipment, and inventory. Damage severity is visualized using a standardized color scale: light amber (<25%), orange (25-50%), red (50-75%), and purple (>75%). Interactive building-level tooltips display sampled flood depth, assigned occupancy code, structure and contents damage percentages, and corresponding monetary losses. Summary statistics report the number of affected buildings, aggregate structural losses, and aggregate contents losses. The interface for infrastructure assessment is illustrated in Figure 14 for a case study in Bellevue, Nebraska.

## 4. Results and Discussion

We highlight the generalization, scalability and applicability of the application through a case study over two affected areas during the 2019 Midwestern flooding events. This case study aims

to showcase the platform's capabilities in real-world disaster scenarios, enabling comparisons against observed flood extents and other inundation mapping platforms.

### 4.1. Case Study: The 2019 Midwestern Floods

The 2019 Midwestern floods represent one of the most significant and widespread flooding events in recent U.S. history, affecting multiple states across the Missouri and Mississippi River basins from March through September. The flooding was triggered by an exceptionally wet spring season, characterized by record-breaking precipitation totals and rapid snowmelt, which created saturated soils and excessive runoff conditions throughout the region (Velásquez et al., 2023). The event resulted in extensive agricultural losses, infrastructure damage, and necessitated numerous flood emergency responses across Iowa, Nebraska, Missouri, and surrounding states (Kraft et al., 2023).

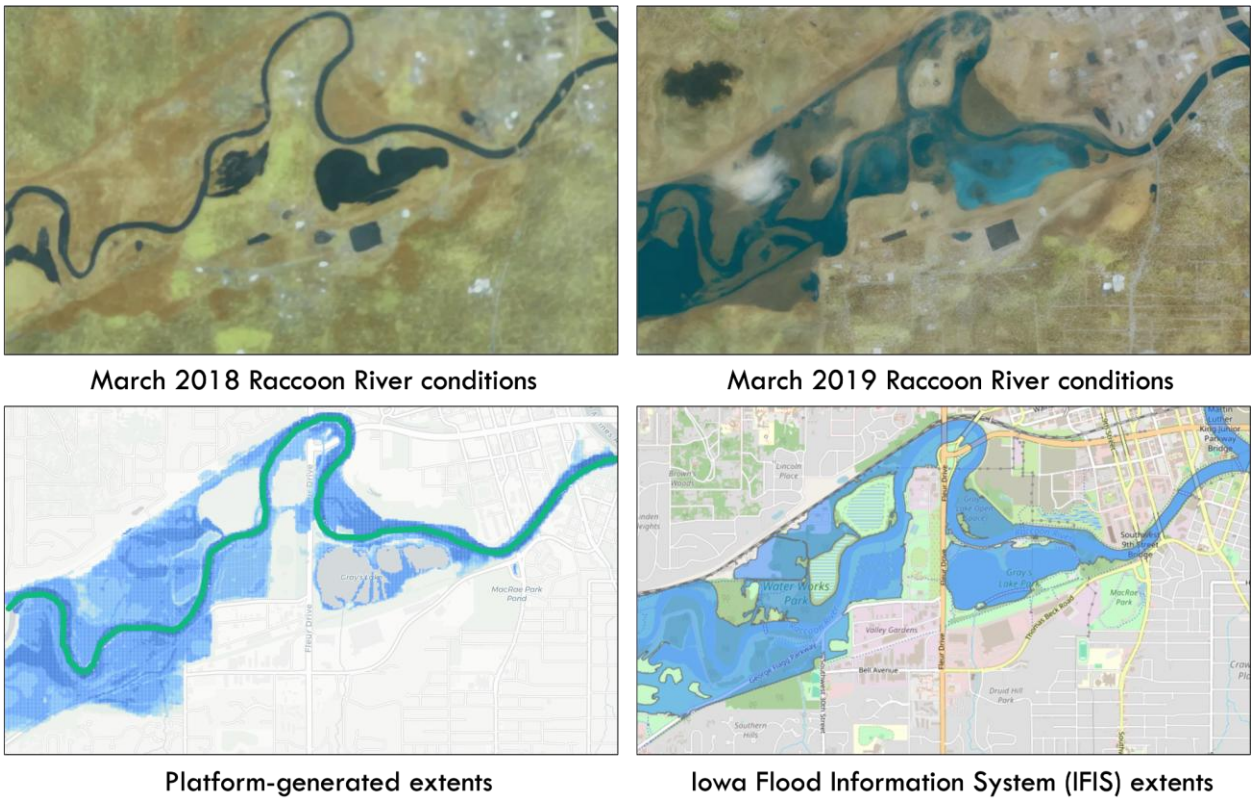


Figure 10. (Top left) Pre-flood satellite imagery from March 2018 displaying normal river conditions; (Top right) Post-flood satellite imagery from March 2019 showing extensive inundation; (Bottom left) Flood extent map generated by the system at 782 cms; (Bottom right) Flood extent map generated by IFIS at 776 cms (Demir & Krajewski, 2013).

This case study examines two representative areas that experienced severe flooding: Des Moines, Iowa, and Bellevue, Nebraska. Two representative HUC-12 watersheds (071000061703 in Des Moines, IA; 102300060603 in Bellevue, NE) were selected to demonstrate the platform's ability to generate flood scenarios. The case study was performed on an M4 MacBook Air with Chrome version 139, Firefox version 142, and Safari version 18.5. All core functionalities

performed as expected across the tested browsers. Minor rendering artifacts were observed in Safari, but did not impair analytical capabilities. This could be attributed to the limited support of newer browser features on Safari (Sabaren et al., 2018).

The Des Moines area serves as a compelling demonstration of the platform's flood mapping capabilities during the 2019 Midwestern floods. The platform successfully captures the spatial patterns of flooding observed in the satellite imagery (NASA Science, 2019b), demonstrating its capability to translate National Water Model discharge predictions into realistic flood extent visualizations through the OWP-FIM methodology. Additionally, the platform's outputs were compared with Iowa Flood Center mapping products for the same flood event. These maps are developed using physics-based hydrodynamic models and validated by the Iowa Flood Center with field observations and high-resolution terrain data (Demir & Krajewski, 2013).

These IFIS maps represent flood conditions in select Iowa communities at half-foot stage intervals. The closest flood map to this study corresponds to a discharge of 776 cubic meters per second. In comparison, the platform-generated maps use 782 cubic meters per second from NWM retrospective data, ensuring similar conditions. Figure 10 displays the comparisons between these maps. These comparisons reveal strong spatial agreement between platform outputs and IFIS products, as well as observed extents. The platform successfully captures flooding patterns along the Raccoon River corridor, including inundation of floodplain areas, recreational zones, and low-lying development areas that experienced flooding during the 2019 event.

### 4.2. Flood Extent Evaluation and HAND Methodology Assessment

The region of interest for testing and evaluating the generated flood extents is Bellevue, Nebraska. This provides an opportunity to evaluate the accuracy of the platform's flood extent predictions, assess the performance of the underlying HAND methodology in representing real-world flood conditions, and test the functionality for assessing infrastructure damage. Before conducting a quantitative comparison, the platform's time-series visualization capabilities were utilized to examine historical discharge during the March 2019 event. Due to limited data availability at stations directly within the Bellevue study area, where monitoring stations were either newly established or lacked complete records during the 2019 flood, time-series analysis was conducted using the USGS gauge station on the Missouri River near Omaha, Nebraska (Figure 11).

This analysis revealed significant discharge magnitudes during the peak flooding period, with USGS observed data showing maximum flows of 5,234 cms, while National Water Model retrospective data estimated approximately 4,000 cms at peak flow. Although such model-observation discrepancies are well-documented in hydrologic forecasting, the platform is flexible, accommodating different discharge sources by accepting user-supplied discharge inputs (e.g., local gauge records, USGS observations, or synthetic hydrographs) to generate inundation maps.

A quantitative assessment of platform-generated flood maps was conducted through a confusion matrix (Townsend, 1971), comparing platform outputs against observed flood conditions during the March 2019 event. We used Landsat Collection 2 Level 3 Dynamic Surface

Water Extent Science Products, obtained from the Earth Resources Observation and Science (EROS) Center (2022), as the reference dataset for a binary flood inundation raster.

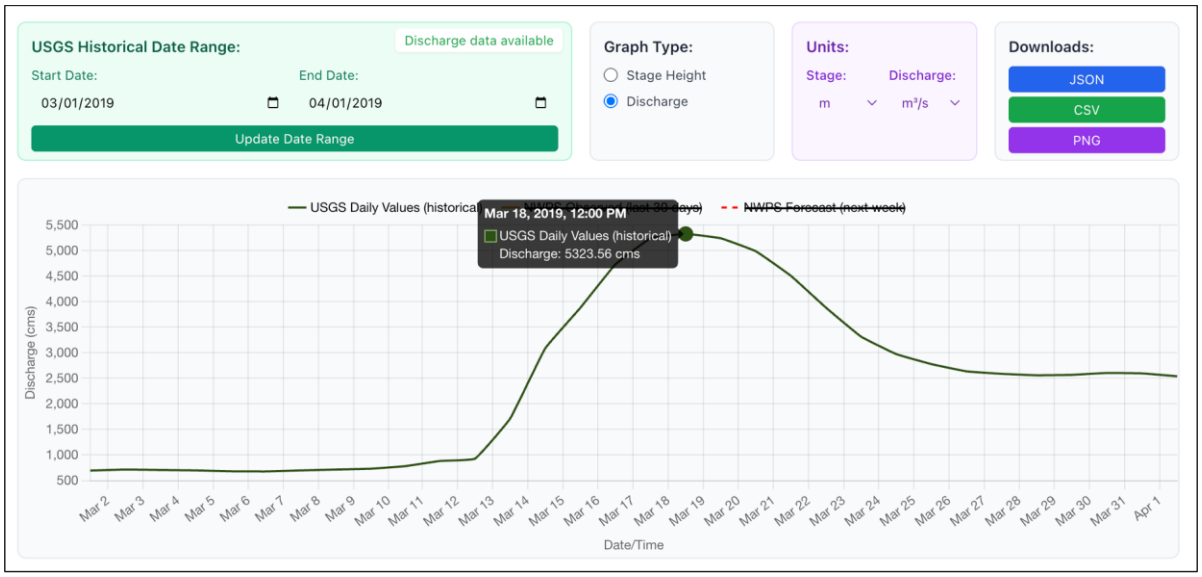


Figure 11. Time-series data for a USGS gauge station (USGS-06610000) in Omaha, NE, near the case study area in Bellevue, Nebraska.

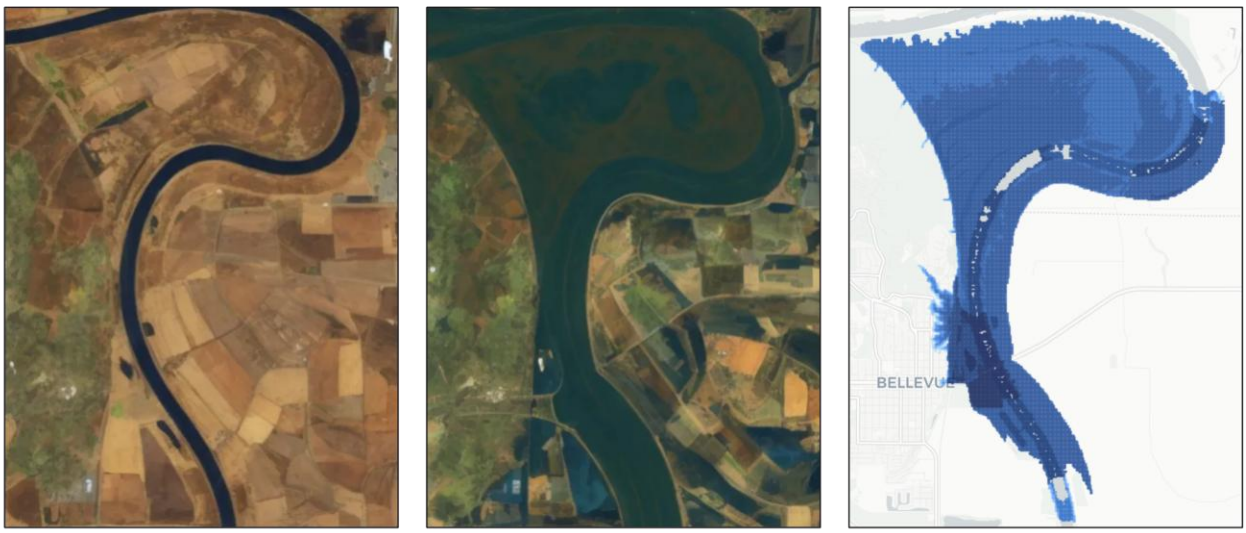


Figure 12. (Left) Satellite imagery for March 20th, 2018, in standard conditions; (Middle) Satellite imagery following the floods, March 16th, 2019; (Right) Flood inundation map generated from the platform, for a river reach near Bellevue, Nebraska (3928 cms).

The validation process involved performing pixel-level alignment between the platform output and the Landsat reference data. Following raster alignment, confusion matrix analysis was conducted to quantify agreement between platform predictions and observed flood conditions

across seven distinct HydroID catchment regions within the study area. Figure 12 illustrates the comparison between 2018 pre-flood conditions, observed 2019 flooding (NASA Science, 2019a), and the platform-generated flood maps.

Platform performance was quantified using Percent Correct, Hit Rate, and Precision metrics to compare generated flood extents against observed conditions. These metrics offer complementary perspectives on flood mapping accuracy by assessing various aspects of prediction quality. True Positives (TP) represent pixels correctly identified as flooded by both the platform and reference data. False Positives (FP) are pixels incorrectly predicted as flooded by the platform but not flooded in the reference data. True Negatives (TN) represent pixels correctly identified as non-flooded by both datasets, while False Negatives (FN) are pixels that were actually flooded but missed by the platform predictions. Percent Correct measures overall accuracy by calculating the proportion of correctly identified pixels relative to the total number of pixels analyzed:

$$Percent\ Correct\ =\ (TP\ +\ TN)\ /\ (TP\ +\ FN\ +\ FP\ +\ TN) \qquad (Eq\ 1)$$

Hit Rate, also known as sensitivity or recall, represents the platform's ability to detect flooded areas correctly:

$$Hit\ Rate\ =\ TP\ /\ (TP\ +\ FN) \qquad (Eq\ 2)$$

Precision quantifies the reliability of flood predictions by measuring the proportion of predicted flooded pixels that were actually flooded:

$$Precision\ =\ TP\ /\ (TP\ +\ FP) \qquad (Eq\ 3)$$

The validation results reveal spatial variability in performance across different catchment areas, as shown in Table 1. The seven catchment areas are illustrated in Figure 13. High-performing regions (B, D, F, G) demonstrate PC values exceeding 92% with consistently high Hit Rates (> 94%) and Precision (> 97%), indicating that the platform effectively captures flood patterns in these regions. While most areas showed high accuracy (PC > 92%), some regions exhibited lower performance. For example, Area C exhibited significant underestimation (PC = 52.40%), a discrepancy attributed to limitations in the source OWP-FIM raster for the main stream channel. Similarly, Area E exhibited moderate overestimation (Precision = 65.79%), likely due to challenges with the underlying model in certain topographic conditions.

This validation exercise demonstrates that the platform can produce flood-inundation maps with a high level of accuracy, supporting their use in practical applications. It enables exploratory analysis across any region of the continental United States. It provides a foundation for operational tasks, including emergency planning, risk communication, and resource allocation during flood events. The results reflect this capability, as five of the seven catchment areas modeled flood extents that closely matched observed extents. Although performance varies by region, the overall

agreement with actual extents indicates the platform can deliver reliable outputs suitable for broader applications.

Table 1. Confusion matrix for comparison between platform-generated and observed extents (TP: True Positive, FP: False Positive, TN: True Negative, FN: False Negative)

| Area | TP (%) | FP (%) | TN (%) | FN (%) | Percent Correct (%) | Hit Rate (%) | Precision (%) |
|---|---|---|---|---|---|---|---|
| A | 88.19 | 2.75 | 0.60 | 8.46 | **88.79** | 91.25 | 96.98 |
| B | 98.96 | 0.43 | 0.13 | 0.48 | **99.09** | 99.51 | 99.57 |
| C | 52.40 | 0.00 | 0.00 | 47.60 | **52.40** | 52.40 | 100.00 |
| D | 76.76 | 0.94 | 18.69 | 3.61 | **95.45** | 95.51 | 98.79 |
| E | 24.21 | 12.58 | 55.71 | 7.50 | **79.91** | 76.34 | 65.79 |
| F | 94.44 | 2.08 | 0.17 | 3.32 | **94.60** | 96.60 | 97.85 |
| G | 92.22 | 2.32 | 0.19 | 5.26 | **92.41** | 94.60 | 97.54 |

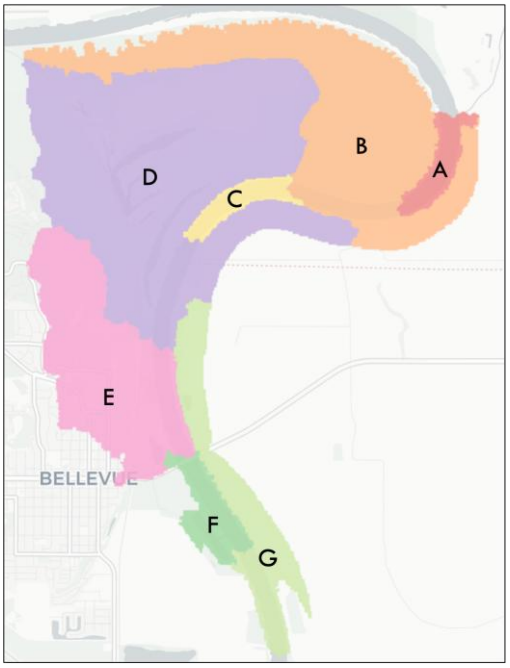


Figure 13. Seven HydroID catchment regions used in the assessment, areas A through G.

### 4.3. Evaluation of Impacted Infrastructure

Focusing on the heavily affected Bellevue region, the platform's infrastructure impact assessment capabilities were demonstrated. The system automatically identified buildings within the flood-affected area and calculated potential structural and content damage based on flood depth and

occupancy classification values. Within the affected area, 169 buildings were identified, resulting in damage estimates totaling $16.7 million for structural damage and $17.3 million for content damage, according to the Hazus framework. The platform's estimate of 169 affected buildings is consistent with emergency management reports, which documented approximately 200 homes impacted by flooding in the Bellevue region (WOWT, 2023). This demonstrates the platform's capability to capture both the spatial extent and general magnitude of flood impacts. The affected structures in the region are highlighted in Figure 14.

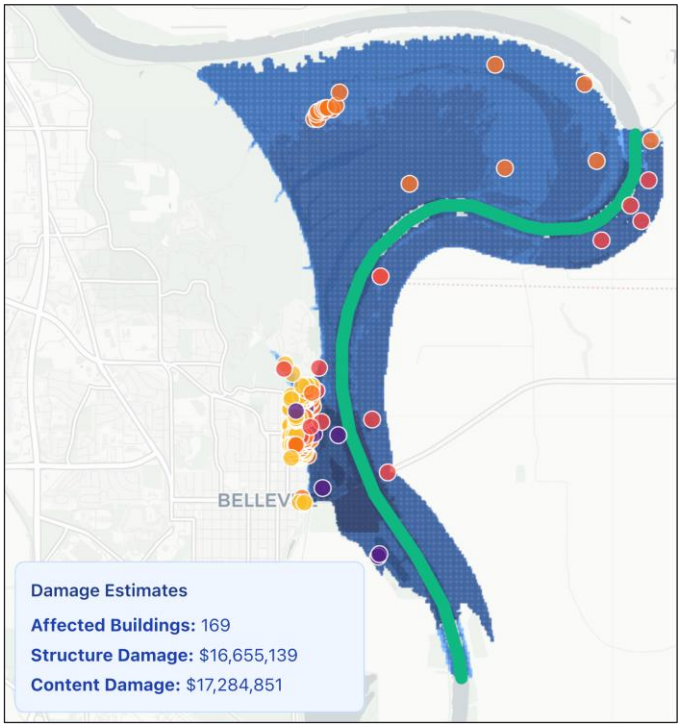


Figure 14. Damage assessment results for Bellevue, Nebraska. Points represent flood-affected structures, colored by damage severity: light amber (<25%), orange (25-50%), red (50-75%), and purple (>75%).

### 4.4. Performance Evaluation and Limitations

The case study results demonstrate that client-side architecture supports responsive, scenario-based flood mapping while maintaining accuracy suitable for emergency planning and preliminary impact assessments. This performance represents a significant advantage, as updating a flood scenario by adjusting discharge or stage on an M4 MacBook Air results in the generation of a new flood map in under one second, a capability made possible by efficient in-browser raster processing. This represents a substantial improvement over traditional desktop workflows and reflects a design optimized for accessibility and rapid assessment, rather than for the complete physical fidelity of detailed hydrodynamic models.

The primary performance bottleneck is rooted in the initial data preparation for a given watershed. This one-time process involves downloading the complete OWP-FIM dataset at the

HUC-8 scale and caching it in the browser with IndexedDB. While this initial download may take several minutes, depending on network conditions, all subsequent analyses within that watershed occur near-instantaneously. The performance characteristics from Bellevue, Nebraska, case study are quantified in Table 2. For these measurements, an M4 MacBook Air with Chrome version 140 was used, with Wi-Fi at a speed of 100 Mbps.

Table 2. Representative performance benchmarks on a modern desktop browser (*Tested on Wi-Fi at 100 Mbps speeds. **Tested on an M4 MacBook Air, Chrome version 140)

| **Operation** | **Time** | **Notes** |
|---|---|---|
| Initial FIM Data Download (336 MB) | 47 seconds* | One-time, network-dependent download per HUC-8. |
| Initial Scenario Generation | 4-8 seconds** | NWM available data call, optimal bounds calculation, raster retrieval, mosaicking, and raster generation. |
| Initial Infrastructure Damage Assessment | 1-2 seconds** | API call and instantaneous calculation for each structure's representative flood depths. |
| Scenario Re-render | <600 ms** | Near instantaneous update through cached data. |

The platform's predictive accuracy is linked to the underlying HAND methodology and the resolution of the source datasets. While the approach provides a computationally efficient alternative for timely assessment, its precision is influenced by factors such as the 10-meter resolution of the source DEM and the use of synthetic rating curves, which may not fully capture local hydraulic variability (Tomkins, 2012). Furthermore, the utility of the platform is dependent on the availability and quality of the federal datasets it integrates. For instance, the completeness of the National Structure Inventory can vary geographically, which may impact the comprehensiveness of damage assessments. From a technical perspective, the client-side architecture requires careful memory management, and performance may vary on older hardware with limited processing power when handling large datasets. Secure and reliable API connectivity is also a consideration for maintaining operational stability.

## 5. Conclusions

This study presents a comprehensive generalized client-side platform for flood inundation mapping and infrastructure impact assessment. By integrating federal datasets from OWP-FIM and NWM within a browser-based architecture, we overcome the accessibility and cost barriers of traditional desktop and server-dependent systems. The 2019 Midwestern floods case study demonstrated the platform's ability to produce flood extents and damage estimates with a high degree of accuracy compared to observed data and official products, showing its effectiveness for real-world scenarios.

The platform performance, analytical scope, and decision-support capabilities can be further enhanced in future studies. For performance, adopting WebGPU could harness client-side graphics

processing units to parallelize raster operations, thereby reducing computation time and enabling the analysis of larger geographic extents. The platform's analytical capabilities could be further enhanced by incorporating additional impact models, such as those for quantifying agricultural losses or modeling disruptions to transportation networks. To better support planning and mitigation efforts, interactive tools will be developed that allow users to simulate interventions, such as proposed levees, and receive immediate visual feedback on how such changes affect flood extents. Finally, to support analyses that exceed the practical limits of client-side processing, a hybrid architecture will be investigated to provide a scalable solution that accommodates both rapid, localized assessments and more extensive, regional-scale studies.

This work demonstrates that web-based flood modeling can serve as a viable complement to traditional approaches, showing that browser-based platforms can achieve sufficient accuracy for practical applications while providing high accessibility. The platform bridges the gap between sophisticated scientific tools and practical decision-support applications, enabling broader stakeholder participation in flood risk assessment and emergency planning. As web technologies advance and federal datasets become more accessible, platforms of this type provide critical tools that support the democratization of hydrological modeling and improve water resources decision-making.

## 6. References


Agafonkin, V. (2020). Geobuf: A compact binary encoding for geographic data. (v.3.0.2) [Software Library]. https://github.com/mapbox/geobuf

Agafonkin, V. (2023). Lefalet: JavaScript library for mobile-friendly interactive maps. (v.1.9.4) [Software Library]. https://github.com/Leaflet/Leaflet

Alabbad, Y., Mount, J., Campbell, A. M., & Demir, I. (2024). A web-based decision support framework for optimizing road network accessibility and emergency facility allocation during flooding. Urban Informatics, 3(1). https://doi.org/10.1007/s44212-024-00040-0

Alabbad, Y., Yildirim, E., & Demir, I. (2023). A web-based analytical urban flood damage and loss estimation framework. Environmental Modelling & Software, 163, 105670. https://doi.org/10.1016/j.envsoft.2023.105670

Aristizabal, F., Chegini, T., Petrochenkov, G., Salas, F., & Judge, J. (2024). Effects of high-quality elevation data and explanatory variables on the accuracy of flood Inundation mapping via height above nearest drainage. Hydrology and Earth System Sciences, 28(6), 1287-1315. https://doi.org/10.5194/hess-28-1287-2024

Aristizabal, F., Salas, F., Petrochenkov, G., Grout, T., Avant, B., Bates, B., Spies, R., Chadwick, N., Wills, Z., & Judge, J. (2023). Extending height above nearest drainage to model multiple fluvial sources in flood Inundation mapping applications for the U.S. national water model. Water Resources Research, 59(5). https://doi.org/10.1029/2022wr032039

Baruah, A., Dhital, S., Cohen, S., Duc Tran, T. N., Elhaddad, H., Watts, C. L., Devi, D., Chen, Y., & Pruitt, C. (2025a). FIMserv v.1.0: A tool for streamlining flood Inundation mapping (FIM)

using the United States operational hydrological forecasting framework. Environmental Modelling & Software, 192, 106581. https://doi.org/10.1016/j.envsoft.2025.106581

Baruah, A., Spies, R., Devi, D., Cohen, S., Aristizabal, F., Nikrou, P., Tian, D., & Pruitt, C. (2025b). Predicting synthetic rating curve adjustment factors with explainable machine learning for enhancing the United States operational flood Inundation mapping framework. Journal of Hydrology, 662, 134086. https://doi.org/10.1016/j.jhydrol.2025.134086

Blodgett, D., & Johnson, M. (2025). Progress toward a reference hydrologic Geospatial fabric for the United States. Water Data For The Nation Blog. https://waterdata.usgs.gov/blog/hydrofabric/

Brakebill, J. W., Schwarz, G. E., & Wieczorek, M. E. (2020). An enhanced hydrologic stream network based on the NHDPlus medium resolution dataset. Scientific Investigations Report. https://doi.org/10.3133/sir20195127

CARTO. (2024). Basemaps. CARTO Documentation. https://docs.carto.com/carto-user-manual/maps/basemaps

Cikmaz, B. A., Yildirim, E., & Demir, I. (2025). Flood susceptibility mapping using fuzzy analytical hierarchy process for Cedar Rapids, Iowa. *International journal of river basin management*, *23*(1), 1-13.

Cosgrove, B., Gochis, D., Flowers, T., Dugger, A., Ogden, F., Graziano, T., Clark, E., Cabell, R., Casiday, N., Cui, Z., Eicher, K., Fall, G., Feng, X., Fitzgerald, K., Frazier, N., George, C., Gibbs, R., Hernandez, L., Johnson, D., … Zhang, Y. (2024). NOAA's national water model: Advancing operational hydrology through continental-scale modeling. JAWRA Journal of the American Water Resources Association, 60(2), 247-272. https://doi.org/10.1111/1752-1688.13184

Demir, I., & Krajewski, W. F. (2013). Towards an integrated flood information system: Centralized data access, analysis, and visualization. Environmental Modelling & Software, 50, 77-84. https://doi.org/10.1016/j.envsoft.2013.08.009

Demiray, B. Z., Sit, M., & Demir, I. (2021). DEM super-resolution with efficientNetV2. *arXiv preprint arXiv:2109.09661*.

Demiray, B. Z., Sermet, Y., Yildirim, E., & Demir, I. (2025). FloodGame: An interactive 3D serious game on flood mitigation for disaster awareness and education. Environmental Modelling & Software, 188, 106418. https://doi.org/10.1016/j.envsoft.2025.106418

DeVries, B., Huang, C., Armston, J., Huang, W., Jones, J. W., & Lang, M. W. (2020). Rapid and robust monitoring of flood events using Sentinel-1 and Landsat data on the Google Earth engine. Remote Sensing of Environment, 240, 111664. https://doi.org/10.1016/j.rse.2020.111664

Dohler, D. (2022). Loam: JavaScript wrapper for GDAL in the browser. (v.1.2.0) [Software Library]. https://github.com/azavea/loam

Dufour, D. J. (2022). GeoTIFF/georaster-layer-for-leaflet: Display GeoTIFFs and soon other types of raster on your leaflet map. (v.3.10.0) [Software Library]. https://github.com/GeoTIFF/georaster-layer-for-leaflet

Earth Resources Observation and Science (EROS) Center. (2022). Landsat Level-3 Dynamic Surface Water Extent, Collection 2 [Dataset]. U.S. Geological Survey. https://doi.org/10.5066/P9DPWBUS

Emiroglu, E., Grant, C. A., Sermet, Y., & Demir, I. (2025). Floodcraft: Game-based interactive learning environment using Minecraft for flood mitigation for K-12 education. International Journal of Disaster Risk Reduction, 130, 105799. https://doi.org/10.1016/j.ijdrr.2025.105799

Erazo Ramirez, C., Sermet, Y., Molkenthin, F., & Demir, I. (2022). HydroLang: An open-source web-based programming framework for hydrological sciences. Environmental Modelling & Software, 157, 105525. https://doi.org/10.1016/j.envsoft.2022.105525

Erazo Ramirez, C., Sermet, Y., & Demir, I. (2023). HydroLang markup language: Community-driven web components for hydrological analyses. Journal of Hydroinformatics, 25(4), 1171-1187. https://doi.org/10.2166/hydro.2023.149

Ewing, G., Mantilla, R., Krajewski, W., & Demir, I. (2022). Interactive hydrological modelling and simulation on client-side web systems: An educational case study. Journal of Hydroinformatics, 24(6), 1194-1206. https://doi.org/10.2166/hydro.2022.061

Gesch, D., Oimoen, M., Greenlee, S., Nelson, C., Steuck, M., & Tyler, D. (2002). The national elevation dataset. Photogrammetric engineering and remote sensing, 68(1), 5-32.

Gorelick, N., Hancher, M., Dixon, M., Ilyushchenko, S., Thau, D., & Moore, R. (2017). Google Earth engine: Planetary-scale geospatial analysis for everyone. Remote Sensing of Environment, 202, 18-27. https://doi.org/10.1016/j.rse.2017.06.031

Hales, R. C., Nelson, E. J., Souffront, M., Gutierrez, A. L., Prudhomme, C., Kopp, S., Ames, D. P., Williams, G. P., & Jones, N. L. (2022). Advancing global hydrologic modeling with the <scp>GEOGloWS ECMWF</scp> streamflow service. Journal of Flood Risk Management, 18(1). https://doi.org/10.1111/jfr3.12859

Horsburgh, J. S., Morsy, M. M., Castronova, A. M., Goodall, J. L., Gan, T., Yi, H., Stealey, M. J., & Tarboton, D. G. (2015). HydroShare: Sharing diverse environmental data types and models as social objects with application to the hydrology domain. JAWRA Journal of the American Water Resources Association, 52(4), 873-889. https://doi.org/10.1111/1752-1688.12363

Hu, A., & Demir, I. (2021). Real-time flood mapping on client-side web systems using HAND model. Hydrology, 8(2), 65. https://doi.org/10.3390/hydrology8020065

IPCC (Intergovernmental Panel on Climate Change). (2023). Technical summary. Climate Change 2021 – The Physical Science Basis, 35-144. https://doi.org/10.1017/9781009157896.002

Johnson, J. M., Munasinghe, D., Eyelade, D., & Cohen, S. (2019). An integrated evaluation of the national water model (nwm)–height above nearest drainage (HAND) flood mapping methodology. Natural Hazards and Earth System Sciences, 19(11), 2405-2420. https://doi.org/10.5194/nhess-19-2405-2019

Jones, K. A., Niknami, L. S., Buto, S. G., & Decker, D. (2009). Federal standards and procedures for the national watershed boundary dataset (WBD). Techniques and Methods. https://doi.org/10.3133/tm11a3

Kraft, L. L., Villarini, G., & Czajkowski, J. (2023). Characterizing the 2019 Midwest flood: A hydrologic and socioeconomic perspective. Weather, Climate, and Society, 15(3), 603-617. https://doi.org/10.1175/wcas-d-22-0065.1

Li, Z., & Demir, I. (2022). A comprehensive web-based system for flood Inundation map generation and comparative analysis based on height above nearest drainage. Science of The Total Environment, 828, 154420. https://doi.org/10.1016/j.scitotenv.2022.154420

Li, Z., Duque, F. Q., Grout, T., Bates, B., & Demir, I. (2023). Comparative analysis of performance and mechanisms of flood inundation map generation using Height Above Nearest Drainage. *Environmental Modelling & Software*, *159*, 105565.

Markert, K. N., Da Silva, G., Ames, D. P., Maghami, I., Williams, G. P., Nelson, E. J., Halgren, J., Patel, A., Santos, A., & Ames, M. J. (2024). Design and implementation of a BigQuery dataset and application programmer interface (API) for the U.S. national water model. Environmental Modelling & Software, 179, 106123. https://doi.org/10.1016/j.envsoft.2024.106123

McCallum, B. E., & Riskin, M. L. (2025). The U.S. geological survey national Streamgage network, 2024. General Information Product. https://doi.org/10.3133/gip252

Miller, J. (2025). Preact: Fast 3kB alternative to React with the same modern API. (v.10.27.1) [Software Library]. https://github.com/preactjs/preact

Moore, R. B., McKay, L. D., Rea, A. H., Bondelid, T. R., Price, C. V., Dewald, T. G., & Johnston, C. M. (2019). User's guide for the national hydrography dataset plus (NHDPlus) high resolution. Open-File Report. https://doi.org/10.3133/ofr20191096

Mostafiz, R. B., Friedland, C. J., Rahman, M. A., Rohli, R. V., Tate, E., Bushra, N., & Taghinezhad, A. (2021). Comparison of neighborhood-scale, residential property flood-loss assessment methodologies. Frontiers in Environmental Science, 9. https://doi.org/10.3389/fenvs.2021.734294

NASA Science. (2019a, March 18). Historic floods inundate Nebraska. NASA Earth Observatory. https://earthobservatory.nasa.gov/images/144691/historic-floods-inundate-nebraska

NASA Science. (2019b, March 19). Icy floodwaters grind through Iowa. NASA Earth Observatory. https://earthobservatory.nasa.gov/images/144696/icy-floodwaters-grind-through-iowa

Nelson, E. J., Pulla, S. T., Matin, M. A., Shakya, K., Jones, N., Ames, D. P., Ellenburg, W. L., Markert, K. N., David, C. H., Zaitchik, B. F., Gatlin, P., & Hales, R. (2019). Enabling stakeholder decision-making with earth observation and modeling data using Tethys platform. Frontiers in Environmental Science, 7. https://doi.org/10.3389/fenvs.2019.00148

NOAA Office of Water Prediction. (2025). Inundation Mapping. GitHub. https://github.com/NOAA-OWP/inundation-mapping

Nobre, A., Cuartas, L., Hodnett, M., Rennó, C., Rodrigues, G., Silveira, A., Waterloo, M., & Saleska, S. (2011). Height above the nearest drainage – a hydrologically relevant new terrain model. Journal of Hydrology, 404(1-2), 13-29. https://doi.org/10.1016/j.jhydrol.2011.03.051

Qian, Q., Edwards, D. J., Zhang, Y., & Haselbach, L. (2024). Improving flood Inundation mapping accuracy using HEC-RAS modeling: A case study of the Neches river tidal floodplain in Texas. Journal of Hydrologic Engineering, 29(4). https://doi.org/10.1061/jhyeff.heeng-6037

Ramirez, C. E., Sermet, Y., & Demir, I. (2024). HydroCompute: An open-source web-based computational library for hydrology and environmental sciences. Environmental Modelling & Software, 175, 106005. https://doi.org/10.1016/j.envsoft.2024.106005

Rebolho, C., Andréassian, V., & Le Moine, N. (2018). Inundation mapping based on reach-scale effective geometry. Hydrology and Earth System Sciences, 22(11), 5967-5985. https://doi.org/10.5194/hess-22-5967-2018

Sabaren, L. N., Mascheroni, M. A., Greiner, C. L., & Irrazábal, E. (2018). A systematic literature review in cross-browser testing. Journal of Computer Science and Technology, 18(01), e03. https://doi.org/10.24215/16666038.18.e03

Samela, C., Albano, R., Sole, A., & Manfreda, S. (2018). A GIS tool for cost-effective delineation of flood-prone areas. Computers, Environment and Urban Systems, 70, 43-52. https://doi.org/10.1016/j.compenvurbsys.2018.01.013

Scawthorn, C., Flores, P., Blais, N., Seligson, H., Tate, E., Chang, S., Mifflin, E., Thomas, W., Murphy, J., Jones, C., & Lawrence, M. (2006). HAZUS-MH flood loss estimation methodology. II. Damage and loss assessment. Natural Hazards Review, 7(2), 72-81. https://doi.org/10.1061/(asce)1527-6988(2006)7:2(72)

Seneviratne, S. I., Zhang, X., Adnan, M., Badi, W., Dereczynski, C., Luca, A. D., Ghosh, S., Iskandar, I., Kossin, J., Lewis, S., Otto, F., Pinto, I., Satoh, M., Vicente-Serrano, S. M., Wehner, M., Zhou, B., & Allan, R. (2021). Weather and climate extreme events in a changing climate. Climate Change 2021: The Physical Science Basis: Working Group I contribution to the Sixth Assessment Report of the Intergovernmental Panel on Climate Change, 1513-1766. https://doi.org/10.1017/9781009157896.013

Sit, M., Sermet, Y., & Demir, I. (2019). Optimized watershed delineation library for server-side and client-side web applications. Open Geospatial Data, Software and Standards, 4(1). https://doi.org/10.1186/s40965-019-0068-9

Sit, M., Langel, R. J., Thompson, D., Cwiertny, D. M., & Demir, I. (2021). Web-based data analytics framework for well forecasting and groundwater quality. *Science of the Total Environment*, *761*, 144121.

Sufi, M., Ramirez, C. E., & Demir, I. (2025). HydroLang FRAM: Web-based framework for comprehensive flood risk and mitigation assessment and communication. International Journal of Disaster Risk Reduction, 128, 105735. https://doi.org/10.1016/j.ijdrr.2025.105735

Sugarbaker, L. J., Constance, E. W., Heidemann, H. K., Jason, A. L., Lukas, V., Saghy, D. L., & Stoker, J. M. (2014). The 3D elevation program initiative: A call for action. Circular. https://doi.org/10.3133/cir1399

Teng, J., Jakeman, A., Vaze, J., Croke, B., Dutta, D., & Kim, S. (2017). Flood Inundation modelling: A review of methods, recent advances and uncertainty analysis. Environmental Modelling & Software, 90, 201-216. https://doi.org/10.1016/j.envsoft.2017.01.006

Thalakkottukara, N. T., Thomas, J., Watkins, M. K., Holland, B. C., Oommen, T., & Grover, H. (2024). Suitability of the height above nearest drainage (HAND) model for flood Inundation mapping in data-scarce regions: A comparative analysis with hydrodynamic models. Earth Science Informatics, 17(3), 1907-1921. https://doi.org/10.1007/s12145-023-01218-x

Tomkins, K. M. (2012). Uncertainty in streamflow rating curves: Methods, controls and consequences. Hydrological Processes, 28(3), 464-481. https://doi.org/10.1002/hyp.9567

Townsend, J. T. (1971). Theoretical analysis of an alphabetic confusion matrix. Perception & Psychophysics, 9(1), 40-50. https://doi.org/10.3758/bf03213026

Trenberth, K. E., Fasullo, J. T., & Shepherd, T. G. (2015). Attribution of climate extreme events. Nature Climate Change, 5(8), 725-730. https://doi.org/10.1038/nclimate2657

Tsegaye, S., Kebedew, M. G., Albrecht, K. K., Missimer, T. M., Thomas, S., & Elshall, A. S. (2024). Integrated GIS-hydrologic-hydraulic modeling to assess combined flood drivers in coastal regions: A case study of Bonita Bay, Florida. Frontiers in Water, 6. https://doi.org/10.3389/frwa.2024.1468354

U.S. Army Corps of Engineers. (2022). National Structure Inventory: Technical documentation. Hydrologic Engineering Center. https://www.hec.usace.army.mil/confluence/nsi/technicalreferences/latest/technical-documentation

Velásquez, N., Quintero, F., Koya, S. R., Roy, T., & Mantilla, R. (2023). Snow-detonated floods: Assessment of the U.S. Midwest March 2019 event. Journal of Hydrology: Regional Studies, 47, 101387. https://doi.org/10.1016/j.ejrh.2023.101387

Wathan, A. (2024). Tailwind CSS: A utility-first CSS framework for rapid UI development. (v.3.4.17) [Software Library]. https://github.com/tailwindlabs/tailwindcss

Wing, O. E., Bates, P. D., Smith, A. M., Sampson, C. C., Johnson, K. A., Fargione, J., & Morefield, P. (2018). Estimates of present and future flood risk in the conterminous United States. Environmental Research Letters, 13(3), 034023. https://doi.org/10.1088/1748-9326/aaac65

WOWT. (2023). Efforts still being made to rebuild Bellevue years after disastrous flood. https://www.wowt.com/2023/11/30/rebuilding-bellevue-after-2019-flood-continues-years-later/

You, E. (2025). Vite: Next generation frontend tooling. (v.6.3.5) [Software Library]. https://github.com/vitejs/vite

## 7. Declaration of AI-Assisted Technologies

During the preparation of this work, the authors used ChatGPT to improve the flow of the text, correct any potential grammatical errors, and improve the writing. After using this tool, the authors reviewed and edited the content as needed and took full responsibility for the content of the publication.

## 8. Appendix

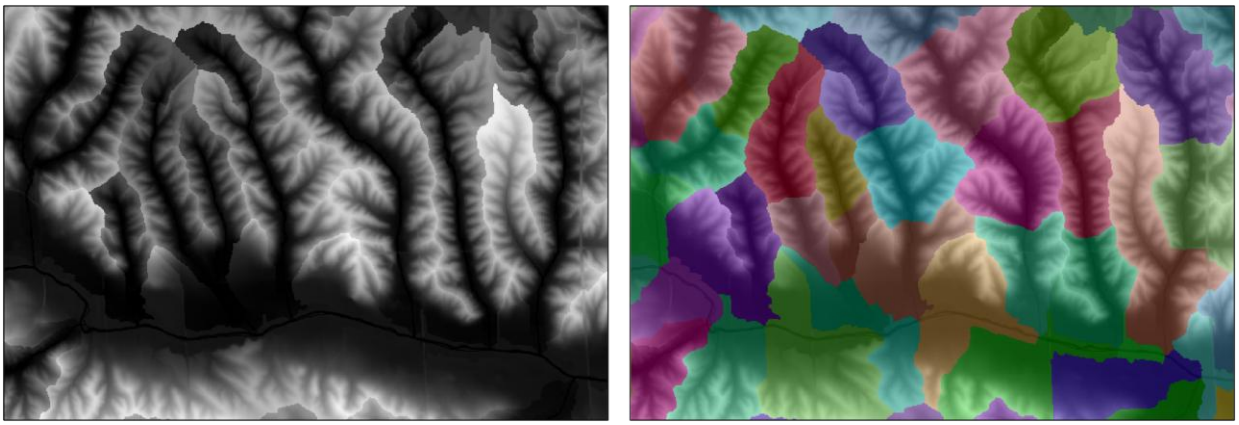

Figure S1. Example of OWP-HAND relative elevation model (left) and HydroID catchments (right).

Table S1. Description of data sources used throughout the study.

| Service Name | Source Description | Platform Integration | Citation |
|---|---|---|---|
| National Water Model (NWM): Retrospective Data | Discharge predictions through retrospective data from 1980 to 2022. | Fetch and display real-time discharge data. | Cosgrove et al., 2024 |
| National Water Model (NWM): BigQuery API | Discharge predictions through data assimilation and short, medium, and long-range forecasts from 2018 to the present. | Fetch and display real-time discharge data. | Markert et al., 2024 |
| National Hydography Dataset Plus (Medium Resolution) | Hydrography for the CONUS, including flowlines and catchments | Displayed flowlines on the map; flood maps are generated at the flowline (COMID) scale | Brakebill et al., 2020 |
| Watershed Boundary Dataset | Watershed boundaries at the HUC-2 through HUC-12. | Displaying catchments through a click-to-expand navigation system. | Jones et al., 2009 |
| USGS 3DEP | Elevation data in 10m resolution and NAVD88 datum. | Elevation display and download. | Sugarbaker et al., 2014 |
| USGS Daily Values | Observed discharge/stage values at USGS stations. | Time-series data visualization | McCallum & Riskin, 2025 |

| | | | |
|---|---|---|---|
| NOAA National Water Prediction Service (NWPS) | Streamflow predictions on select USGS stations. | Time-series data visualization | Cosgrove et al., 2024 |
| OWP Flood Inundation Mapping (OWP-FIM) | Relative elevation model (REM) and rating curves for flood inundation mapping at the HUC-8 scale. CIROH provides a public mirror of the AWS bucket. | Flood inundation layer on the map and download. | NOAA Office of Water Prediction, 2025 |
| FEMA Hazus Damage Curves | Formulas for building damage based on flood depth and occupancy types. | Damage calculations for scenario-based inundation extents. | Scawthorn et al., 2006 |
| USACE National Structure Inventory (NSI) | Dataset for properties in the United States, with structure and content value estimates. | Damage calculations for scenario-based inundation extents. | U.S. Army Corps of Engineers, 2022 |

Table S2. Abbreviations of the terms used in the paper.

| **Abbreviation** | **Definition** |
|---|---|
| API | Application Programming Interface |
| AWS | Amazon Web Services |
| CIROH | Cooperative Institute for Research to Operations in Hydrology |
| COG | Cloud Optimized GeoTIFF |
| COMID | Common Identifier |
| CSS | Cascading Style Sheets |
| DEM | Digital Elevation Model |
| EPSG | European Petroleum Survey Group |
| FEMA | Federal Emergency Management Agency |
| FIM | Flood Inundation Mapping |
| FN | False Negatives |
| FP | False Positives |
| GDAL | Geospatial Data Abstraction Library |
| GIS | Geographic Information Systems |
| HAND | Height Above Nearest Drainage |
| HAZUS | Hazards U.S. |

| | |
|---|---|
| HUC | Hydrologic Unit Code |
| IFIS | Iowa Flood Information System |
| IndexedDB | Indexed Database |
| JSON | JavaScript Object Notation |
| LiDAR | Light Detection and Ranging |
| ML | Machine Learning |
| NAD83 | North American Datum 1983 |
| NAVD88 | North American Vertical Datum 1988 |
| NHD | National Hydrography Dataset |
| NOAA | National Oceanic and Atmospheric Administration |
| NSI | National Structure Inventory |
| NWM | National Water Model |
| NWPS | National Water Prediction Service |
| OWP | Office of Water Prediction |
| OWP-FIM | Office of Water Prediction Flood Inundation Mapping |
| PC | Percent Correct |
| PNG | Portable Network Graphics |
| PostGIS | Spatial Database Extender for PostgreSQL |
| PostgreSQL | Open Source Relational Database |
| RAM | Random Access Memory |
| REM | Relative Elevation Model |
| SRC | Synthetic Rating Curve |
| TIF | Tagged Image File Format |
| TN | True Negatives |
| TP | True Positives |
| USACE | U.S. Army Corps of Engineers |
| USGS | United States Geological Survey |
| WASM | WebAssembly |
| WFS | Web Feature Service |
| WGS84 | World Geodetic System 1984 |